REVIVING MEDIEVAL MECHANISMS: DESIGN STUDY OF MECHANICAL ESCAPEMENTS FOR USE IN SPACE

What Parameters Influence Performance and How To Predict It

Abstract

This paper explores the feasibility of harnessing a 13th-century mechanical escapement to address challenges of the 21st-century. The primary objective is to evaluate the potential of utilizing this escapement to regulate the deployment velocity of solar arrays in space, within constraints of limited mass and cost-effectiveness, while emphasizing system simplicity. The approach involves a parameter analysis conducted through numerical and analytical modelling, complemented by prototype-based performance testing to validate our models. The results of the research indicate that the verge escapement mechanism is well-suited for this application, and its performance can be reliably predicted through analytical modelling techniques.

Paul B. Heineman

Faculty of Engineering Technology
Department of Precision Mechanics

Committee Chair:	Prof. Dr. Ir. D.M.Brouwer
UT Supervisor:	Dr. Ir. J.J. de Jong
Airbus Supervisor:	Ir. R. Foekema
External Committee Member:	Dr. Ir. M. Ellenbroek

16-11-2023

UNIVERSITY OF TWENTE. AIRBUS

Page Intentionally Left Blank

Table of Contents

Design Study Of Mechanical Escapements For Use In Space using ADAMS, Impulsive Differential Equations and Performance tests.

Paul B. Heineman

1. Introduction

1.1. Solar arrays

Solar arrays for spacecraft are usually manufactured from rigid composite panels covered in photovoltaic cells. These rigid arrays are divided in multiple segments, folded and later deployed in space. This way, it offers protection for the solar cells during launch, since the system is more rigid when stored and held against the spacecraft. In space, this rigidity is no longer necessary so the array can be deployed in its operation configuration.

On Figure 1, a standard solar array configuration can be seen with two wings (1), consisting of three panels (2). These two wings are attached to a dummy spacecraft (3). On the right side of the figure, a folded stack is displayed.

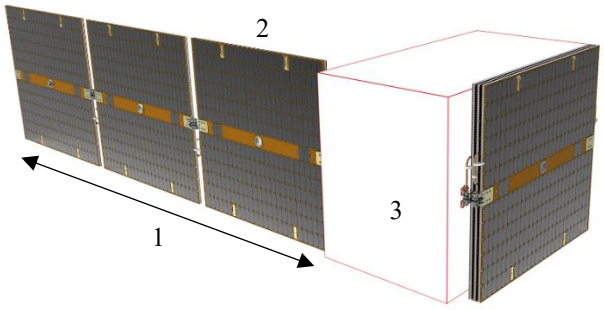

Figure 1 - common solar array layout - source: Airbus NL

One of the options to power this deployment is to use torsions springs on all the hinges. Which means the position of individual panels is not controlled and builds angular velocity over time until the hinges reach the end of their allowed travel. This can result in large moments, called latch shock, on all hinges. This is a manageable problem for small arrays and resilient spacecraft. Wings with a larger number of panels would benefit from a solution that reduces the latch shock and gives some control or predictability to the position of the panels during deployment.

In this paper, the possibility to control the rotational velocity is investigated. In particular for a Sparkwing array as designed by Airbus NL.

1.2. Methods for Velocity Control

Historically, a few methods have been used to reduce the rotational velocity during deployment. The most popular methods discussed here are:

- Escapement
- Eddy Current Damper
- Hydraulic Damper
- Electro Magnetic Damper

1.2.1. Escapements

In clocks, energy is stored in springs. This energy is slowly released by escapements. The escapements allow the clock to provide accurate timekeeping. There are many escapement concepts, two of which are visible in Figure 2. A version of such a mechanism has already been used in space, in the MIRAS deployable antenna onboard the SMOS (Nunez, et al., 2003). The product used there, would be unsuitable for use on a Sparkwing array due to its size and weight. The concept used is an anchor escapement (Figure 2b) together with a gearbox. Another option is the verge escapement (2a) which has not been used in spacecraft before. In clocks, the verge was one of the first escapements to be used for clocks. Later, the anchor provided more accurate timekeeping, however, the verge is predictable enough for this intended use.

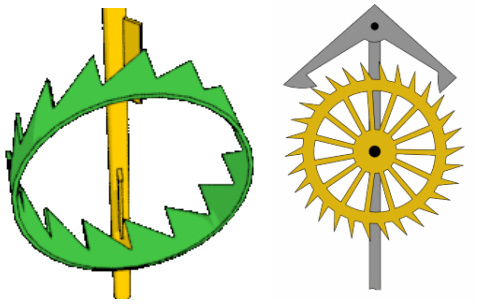

(a) *(b)*

Figure 2 (a) verge Escapement, (b) Anchor Escapement – source: wikipedia

1.2.2. Eddy Current Damper

An eddy current damper is a device that uses electromagnetic induction to generate opposing currents, or eddy currents, in a conductive material, which produces a resistive force that dampens the velocity of the mechanism. This technology is commonly used in various applications, such as train brakes and vibration isolation systems, to reduce unwanted vibrations and oscillations. This system is also currently used on large solar arrays built by Airbus NL (Doejaarden & Ellenbroek, 2012). The cost of this system is relatively high. Because of the high ratio of the gearbox, a slight variation in friction results in large variations in start-up torque. Testing and getting it qualified is therefore resource intensive. This makes the system a significant part of the cost of solar arrays and also unsuitable for smaller, low cost, solar arrays.

1.2.3. Hydraulic dampers

Hydraulic dampers use hydraulic fluid in a housing. When the system experiences movement, the fluid is passed through valves or openings inside the housing. This creates resistance, which can be used to control motion, such as in shock absorbers in cars. The biggest downside of this method is that the temperature in space can vary widely, which has a large nonlinear effect on the damping rate through the viscosity of the hydraulic fluid. This in turn makes the damper unpredictable, or requires complicated mechanisms or actively controlled electromagnets to counteract this change in viscosity (United States of America Patentnr. 5,921,357, 1997).

1.2.4. Electric DC motors.

Finally, brushed DC motors can be used as dampers. This has already been studied as in a paper from 2018 by H.R. Ali-Akbari (Ali-Akbari, 2018). This shows that the damper could be made passive and adjusted to the desired performance. It is not mentioned how high the start-up torque is for that system.

While all methods of controlling the deployment mentioned could be applied, in this paper, the potential of the escapement in this application is investigated.

1.3. Goals and Outline

The goal of this research is to assess the possibilities to use an escapement for controlling the deployment of solar arrays. Therefore the research questions is formulated as follows:

- Can a mechanical escapement of the mass and volume suitable for a Sparkwing array, be used to control solar array deployment on spacecraft?

In order to answer this questions, some additional supporting questions were formulated to guide the research.

- Which parameters dominate the dynamic behaviour of the escapement?
- Can those parameters be used to tailor the escapement to the variation of solar arrays it can encounter? (ex. Variation in torque)
- Can analytical and numerical models accurately predict real world behaviour, considering production accuracy and tolerances?

This paper describes a development process for a verge escapement that can control the rotational velocity of solar array deployment in space. To do that, requirements for such a system are listed and the features impacting rotational velocity of verge escapements are investigated. The development of an analytical model and prototype test plan of the mechanism is described in chapter two. The results coming from the analytical, numerical, and prototype measurements are discussed in chapter four. Finally, the research questions are answered and discussed in the conclusions.

2. Methods

To answer the main research question, it important to understand what constitutes a successful design. For this, the main requirements are mentioned. Afterwards the working principles of the Verge escapement is explained in more detail.

Then, numerical and analytical methods used to predict the behaviour of the escapement are presented. Finally, the test plan of a physical prototype is described.

2.1. Requirements

To control the deployment of the solar arrays, the rotational velocity should be between 0.16 and 1.5 Rotations per minute. In other words, the 90 degree rotation of the first hinge should take between 10 and 90 seconds. The mechanism should not fail during the testing and verification phase, meaning around 200 deployments (Kroon, 2022). Also important, is the volume of the escapement, which should fit within a cylinder with a diameter of 40mm and a length of 100mm. Other requirements are less relevant and can be found in appendix 6.1.

2.2. The Escapement

To give context to the analytical models, which are introduced later in this chapter, it is helpful to get to know the escapement. The way it works and the various phases of its limit cycle are explained. The requirements directed the decisions made during the concept choice, this is also explained in this subsection

2.2.1. The Escapement Choice

As mentioned in the introduction, escapement method of rotational velocity control is considered for this paper. Since the mechanism should be self-starting, function without gravity and fit in the assigned volume, a few options remain. Especially the fact that many escapements rely on a pendulum and therefore gravity, reduces the amount of concepts to consider. The best candidates due to the requirements are the anchor and verge-foliot escapement which were also mentioned in the introduction.

Both the Anchor and the Verge escapement consist of a gear and an oscillating body. In Figure 2, for the verge escapement, the gear is the green body while the oscillating body, called the verge, is in yellow. The Anchor escapement has the gear in yellow and the oscillating body in grey, called the anchor. When torque is applied to the crown gear, the verge/anchor starts oscillating. This process is explained later in more detail. For now, the important fact to know is that the escapements reduce the rotational velocity by controlling the release of energy from the torque source, usually a spring.

To achieve enough control, the movement of the solar panel relative to the spacecraft has to be sped up using a gearbox before the torque is transferred to the crown gears. This gearbox makes that both escapement concepts can apply enough control to reach the required rotational velocity.

For the amount of cycles and the volume requirements however, the verge escapement turns out to be preferable. In Figure 2, it can be seen that the verge fits within the diameter of the crown gear. The anchor sits outside the diameter of the its crown gear. This means that when both escapements have to fit within the 40mm diameter requirement. The crown gear of the verge can be of larger diameter than for the anchor escapement.

This larger diameter allows more gear teeth on the circumference, resulting in more interactions every rotation, spreading wear over more teeth and less contact force for each interaction. Overall, the Verge-Foliot escapement seems the better suited option and is considered for the remainder of this paper.

2.2.2. Verge Escapement

The verge-foliot escapement (Figure 3) was the first escapement used in mechanical clocks. The crown gear and verge allowed for slow release of the energy in the clock spring or weight since only 1 tooth can be released for every cycle. The rate at which the cycles repeat can be changed by adjusting the inertia of foliot (foliot visible on top of the verge indicated with (2)). The escapements of the 13th century were inaccurate due to the short clock springs used, the absence of pendulum and thermal expansion of the foliot, impacting its inertia. The difference at the end of the day could be in the order of hours, so clocks back then only had an hour hand. Many Verge escapements were later adapted to include a pendulum instead of a foliot to increase accuracy (Cipolla, 2003). The pallets are named ‘upper’ and ‘lower’ because historically, the verge was always placed vertically.

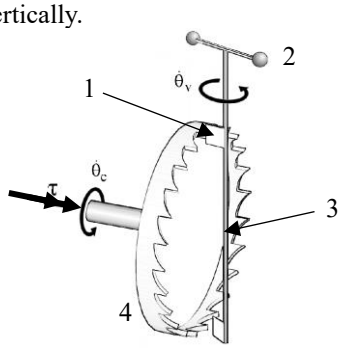

Figure 3 Crown gear (4) and Verge (3) with Foliot (2) on top and two pallets (1). Torque τ, rotational velocities of the crown gear $\dot{\theta}_c$ and verge $\dot{\theta}_v$ are indicated. (Roup & al., 2001)

2.2.3. Motion Phases

The movement of the mechanism can be divided in six distinct phases. The phases are:

1. Simultaneous acceleration (upper)
2. Single acceleration (upper)
3. Collision (lower)
4. Simultaneous acceleration (lower)
5. Single acceleration (lower)
6. Collision (upper)

The phases are described in pairs, since they are the same apart from being mirrored. The phases can be seen in pairs side by side in Figure 4.

Phase 1 and 4

In the first and fourth phase, the torque applied to the system accelerates the crown gear together with the verge since the two parts are in contact. Parts in contact with each other are colored red.

The rate of acceleration is determined by:

- Inertia of verge and crown gear
- Radius of crown gear
- Point of contact on pallet
- Torque applied
- Friction

The duration of the contact is determined by:

- Length of pallets
- Distance between the verge and the top of the teeth

Phase 2 and 5

In the second and fifth phase, the torque only accelerates the crown gear. This means an increase in rate of acceleration of the crown gear compared to the previous phase. Parts that just lost contact are colored red.

Rate of acceleration is determined by:

- Inertia of crown gear
- Input torque
- Friction

The duration of the phase is determined by:

- Length of pallets
- Distance between the verge and the top of the teeth

Phase 3 and 6

In the third and sixth phase, a collision happens between the verge and the crown gear. The particular pallet involved in this collision is moving in opposite direction relative to the crown gear tooth involved. This means a reduction in angular velocity for both components. The velocity after the collision is the input for the phases one and four. Parts involved in the collision are colored red in Figure 4, bottom row. Arrows indicate their direction just before collision.

The velocity after the collision is the input for the phases one and four and is dependent on the following:

- Energy lost in the collision (material & geometry)
- Inertias of crown gear and verge
- Velocities before the collision

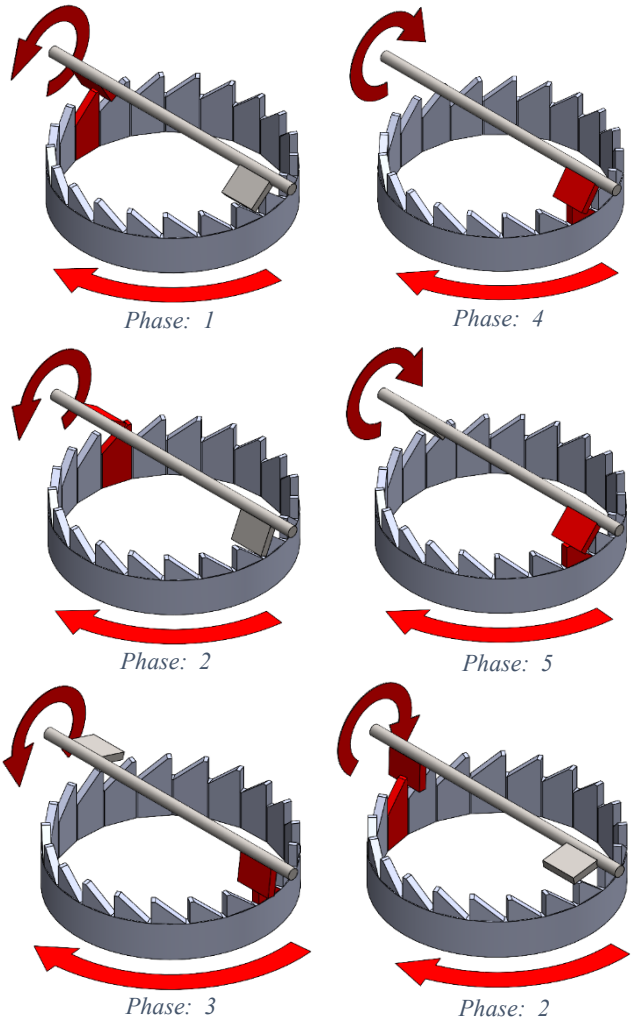

Figure 4 Motion phases

2.3. 2D analytical model

Analysis of the phases described in the previous section can be done using a numerical simulation program such as ADAMS. This software package is suitable for detailed multibody dynamics analysis in the final stages of design. For iteration early in the design process it is more convenient to have a quick calculation to estimate the performance. Therefore, a 2d analytical approach was developed, which will be explained in this section.

The analytical model is based on the work of Alexander Roup (Roup & al., 2001). They analysed the dynamics of the verge and foliot by using impulsive differential equations and they consider phases two, three, five and six. Their analysis uses expressions obtained by (Lepschy, Mian, & Viaro, 1992) and expanded upon their work. This resulted in a detailed dynamic model of the verge and foliot system, from now on called the "Roup-model", using impulsive differential equations. It was shown that these equations could be used to describe the dynamics of the verge foliot system quite well. An expression is formulated for average angular velocity of the crown gear, accurately predicting that velocity is part of the main goal for this paper.

2.3.1. Impulsive differential equations

The model is expanded upon to implement phase one and four, and this new model will from now on be called 'Extended model'. It consists of continuous steps calculated during the acceleration phase (one, two, four and five) and discrete steps in rotational velocity that happen during the collisions in phase three and six. The expansion also allows for the following variables to be integrated in the model:

Distance between verge and crown gear
Spring torque decreasing over time
Phase 1 and 4

During the calculation, the position and velocity of the crown gear and verge is calculated and stored in the state vector $x(t)$ (Equation 1). This vector contains the position and velocity of the crown as x_1 and x_3. Where position x_1 equals the amount the gear has rotated since the initiation. x_3 equals the current angular velocity. The position and velocity of the verge is stated as x_2 and x_4. Where x_2 is the position of the centreline of the verge compared to the vertical, and x_4 is the angular velocity. Meaning that if α_v is the angle between the two pallets, the position of the upper and lower pallets are $x_2 + \frac{1}{2}\alpha_v$ and $x_2 - \frac{1}{2}\alpha_v$ respectively. x_1 and x_2 are visible in Figure (5).

$$x = [x_1 \quad x_2 \quad x_3 \quad x_4]^T \triangleq [\theta_c \quad \theta_v \quad \dot{\theta}_c \quad \dot{\theta}_v]^T \tag{1}$$

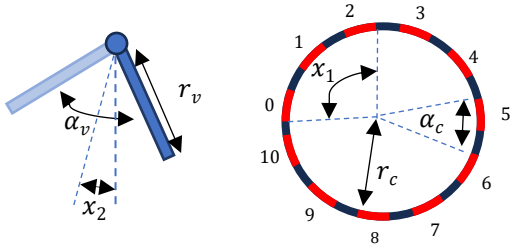

(a) (b)

Figure 5 (a) represent the verge with radius r_v, angle α_v between pallets and position x_2 indicated. (b) represents a top view of the crown gear, with the teeth indicated in red, numbered clockwise, rotation direction counterclockwise. Radius r_c, angle α_c between teeth and position x_1 are indicated.

The method of calculating the state is different for each phase. To assess which phase the mechanism is in, two sets of requirements are checked. The results of these checks determine the active phase. Phase one, two, four and five use continuous-time differential equations representing the acceleration phases of the limit cycle. In phase three and six, the system experiences a discrete step in velocity, this is done using an impulse function.

Phase one and four

For phase one and four, the verge and crown gear should be in contact with each other. This is checked using the contact requirements C_{upper} and C_{lower} seen in Equation (2) and (3). Using these, it is checked if the distance that the pallet extends towards the gear is more than the distance between the axle of the verge and the tip of the gear teeth (h_v). If the pallet does extend that far down, so C is true, contact is possible and the model assumes the two parts are in contact. Obviously, at all times, one of the statements is true since the pallets are angled such that there is no free rotation of the crown gear possible. Therefore, Equation (3) is checked in phase one to see if it needed to progress to phase two, and Equation (4) is used similarly in phase four.

$$C_{upper} = \left\{ r_v \cos\left(x_2 + \frac{\alpha_v}{2}\right) > h_v \right\} \tag{2}$$

$$C_{lower} = \left\{ r_v \cos\left(x_2 - \frac{\alpha_v}{2}\right) > h_v \right\} \tag{3}$$

When in phase one or four, the change in position and velocity between the current and next timestep is calculated according to Equation (4). There, τ represents the torque on the crown gear, and τ_{eff} the effective torque on the verge, exerted by the crown on the verge. I_{eff} and I_v are the effective inertia of both components at the axle of the crown gear and the inertia of the verge respectively.

$$\dot{x}(t) = \begin{bmatrix} 0 & 0 & 1 & 0 \\ 0 & 0 & 0 & 1 \\ 0 & 0 & 0 & 0 \\ 0 & 0 & 0 & 0 \end{bmatrix} \begin{bmatrix} x_1 \\ x_2 \\ x_3 \\ x_4 \end{bmatrix} + \begin{bmatrix} 0 \\ 0 \\ \tau/I_{eff} \\ \tau_{eff}/I_v \end{bmatrix} \tag{4}$$

Phase two and five

When the crown gear loses contact with the verge and condition C becomes false, a different expression for $\dot{x}(t)$ is needed (Equation 5). Now, I_c is used for the crown gear inertia, since only the inertia of the crown gear has to be taken into account. This means that the rate of acceleration increases for the crown gear in this phase. The verge does not accelerate in this phase.

$$\dot{x}(t) = \begin{bmatrix} 0 & 0 & 1 & 0 \\ 0 & 0 & 0 & 1 \\ 0 & 0 & 0 & 0 \\ 0 & 0 & 0 & 0 \end{bmatrix} \begin{bmatrix} x_1 \\ x_2 \\ x_3 \\ x_4 \end{bmatrix} + \begin{bmatrix} 0 \\ 0 \\ \tau/I_c \\ 0 \end{bmatrix} \tag{5}$$

Phase three and six

Phase three and six represent the discrete steps in rotational velocity during the collisions. The phases are triggered by the requirements stated in Equations (6) to (9). These requirements check if the verge and crown gear started making contact and if the two parts are moving towards each other. The latter is needed to prevent the impulse from triggering directly after the previous collision. There are four different sets of requirements, for following four situations:

Upper pallet makes contact with the tip of the verge (Equation 6)(Figure 6a)
Upper pallet makes contact with the tip of a tooth (Equation 7)(Figure 6b)
Lower pallet makes contact with the tip of the verge (Equation 8)(Figure 6a)
Lower pallet makes contact with the tip of a tooth (Equation 9)(Figure 6b)

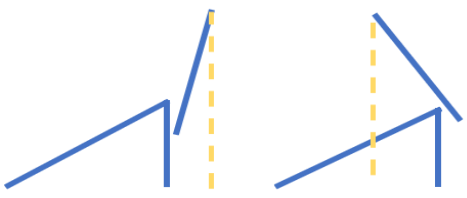

(a) (b)

Figure 6 two possibilities of how the verge and crown gear tooth are positioned during collision

For these equations it is important to know which teeth is in contact. The teeth are numbered from 0 to n, where n is always even, since the crown gear has to have an uneven number of teeth for the mechanism to function correctly (Roup & al., 2001). m represents the teeth in contact. p equals the amount of full turns the crown gear has made. All other variables are indicated in Figure (5).

$$\mathcal{S}_m^{upperpre} = \begin{Bmatrix} x: r_c \sin(x_1 - m\alpha_c) = h_v \tan(x_2 + \alpha_v/2), \\ r_c x_3 - r_v x_4 > 0, (m - 1/2)\alpha_c + 2p\pi \\ \leq x_1 \leq (m + 1/2)\alpha_c + (2p - 1)\pi \end{Bmatrix} \quad (6)$$

$$\mathcal{S}_m^{upperaft} = \begin{Bmatrix} x: r_c \sin(x_1 - m\alpha_c) = r_v \sin(x_2 + \alpha_v/2), \\ r_c x_3 - r_v x_4 > 0, (m - 1/2)\alpha_c + 2p\pi \\ \leq x_1 \leq (m + 1/2)\alpha_c + (2p - 1)\pi \end{Bmatrix} \quad (7)$$

$$\mathcal{S}_m^{lowerpre} = \begin{Bmatrix} x: r_c \sin(m\alpha_c - x_1) = h_v \tan(-x_2 + \alpha_v/2), \\ r_c x_3 + r_v x_4 > 0, (m - 1/2)\alpha_c + (2p - 1)\pi \\ \leq x_1 \leq (m + 1/2)\alpha_c + (2p - 1)\pi \end{Bmatrix} \quad (8)$$

$$\mathcal{S}_m^{loweraft} = \begin{Bmatrix} x: r_c \sin(m\alpha_c - x_1) = r_v \sin(-x_2 + \alpha_v/2), \\ r_c x_3 + r_v x_4 > 0, (m - 1/2)\alpha_c + (2p - 1)\pi \\ \leq x_1 \leq (m + 1/2)\alpha_c + (2p - 1)\pi \end{Bmatrix} \quad (9)$$

When one of the requirement sets is met, the jump function is triggered (Equation 10) (Roup & al., 2001). This calculates the jump in velocity both components of the mechanism make. The expression contains the coefficient of restitution c_r which is explained in the next subsection. The coefficient σ differentiates the collisions at the upper and lower pallet.

$$f_d(x) = \begin{bmatrix} 0 & 0 & 0 & 0 \\ 0 & 0 & 0 & 0 \\ 0 & 0 & -r_c G_c & \sigma r_v G_c \\ 0 & 0 & \sigma r_c G_v & -r_v G_v \end{bmatrix} x \quad (10)$$

Where

$$G_c \triangleq \frac{(I_v/{r_v}^2)(1 + c_r)}{r_c((I_v/{r_v}^2) + (I_c/{r_c}^2))}, \qquad G_c \triangleq \frac{(I_c/{r_c}^2)(1 + c_r)}{r_v((I_v/{r_v}^2) + (I_c/{r_c}^2))} \quad (11)$$

And

$$\sigma \triangleq \begin{cases} +1, & upper\ pallet \\ -1, & lower\ pallet \end{cases} \quad (12)$$

2.3.2. Coefficient of restitution

The coefficient of restitution is defined as a value between 0 and 1, that describes the level of elasticity in a collision between body a and b. 0 would mean a inelastic collision and 1 an elastic collision. This value relates the linear velocities before and after a collision according to the following expression:

$$V_{a1} - V_{b1} = -c_r(V_{a0} - V_{b0}) \quad (13)$$

Where V_{a1} and V_{b1} are the velocities after the collision, and V_{a0} and V_{b0} are the velocities before the collision. In reality this value describes the amount of energy lost due to damping in the form of heat, sound, wear or vibrations and is somewhere in between 0 and 1. (Weir & McGavin, 2008)

2.4. Escapement Design

The analytical model described in the previous section has to be verified using numerical simulations and prototype testing. For both the ADAMS simulations and the manufacturing of a prototype, a 3D model of the escapement is needed. This design is described in this section.

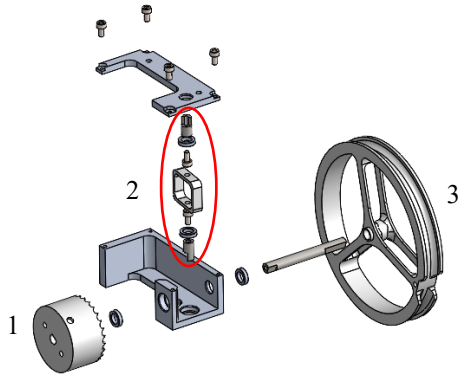

Figure 7 Exploded view of the prototype assembly with the crown gear (1), the verge (in parts) (2) and the wheel that powers the mechanism on the right (3).

Geometry

As explained in subsection 2.2.1, maximizing the diameter of the crown gear is important in order to maximize the reduction of the speed of deployment. The gearbox and mechanism are attached in line to the hinge, the mechanism housing is mounted to the gearbox housing. The crown gear is directly attached to the outgoing shaft of the gearbox. To maximise the diameter of the crown gear, its axle runs through the centre of the verge. The teeth are then oriented towards the gearbox and the verge is located in between the crown gear and the gearbox. This way, the bearings of the verge are inside the crown gear diameter (Figure 8a). This is opposed to having the bearing housing of the verge going around the crown gear and therefore having the crown gear between the verge and the gearbox (Figure 8b). This would reducing the maximum possible diameter of the crown gear.

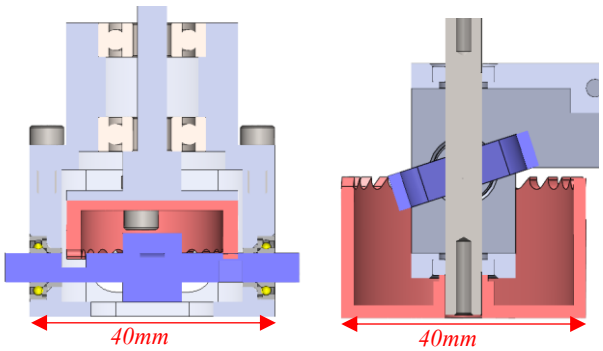

(a) (b)

Figure 8 Normal and section view of the two mechanism arrangements for the crown gear (red) and verge (blue), with a 28mm crown gear for the initial design and a 40mm escape gear for the next iteration. Both variants would attach to gearbox in the top of the figure to the shaft.

2.4.1. Materials

The crown gear will be made out of a technical polymer such as PEEK. This material has a high yield stress and can be machined very well. The verge will be made out of a material with greater hardness and density. Early calculations using Hertzian contact theory showed that this resulted in lower contact stresses. But there are more benefits from this material choice:

More contact damping
: This extracts energy from the system in the form of heat due to deflection of the polymer.

Possibility to concentrate wear on the crown gear
: The pallets experiences much more collisions than the teeth.

Higher density in the verge
: Better performance of the mechanism (see Chapter 3)

The choice of material is important for the coefficient of restitution in the analytical models, and the contact parameters in the numerical model.

2.4.2. Manufacturing

The verge (Figure 7, 9a) becomes quite a complicated part to manufacture due to the crown gear shaft running through the middle of it and the two cylindrical pallets that sit in the bearings. The two pallets have to be slotted into the connecting piece to line up their angle and prevent them from rotating under load. They can still be made quite easy on a lathe and mill albeit precision work. The connecting piece can be made on a conventional mill, but it might be beneficial to 3D print these parts in metals and afterwards machine the bearing surfaces down for the production version.

The crown gear (Figure 9b) was designed with a maximum of 27 teeth to ensure the part stays machinable with a 3mm ball nose milling bit. Since that bit was assumed to be the a small but reasonable bit to be used. A keyway has to be machined to prevent the part from freely rotating around the shaft and if the end of the 6mm shaft is threaded, A bolt and washer there can prevent the gear from moving axially.

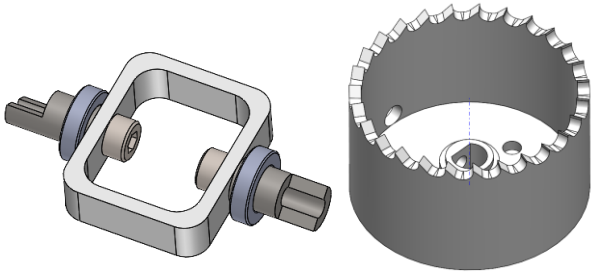

(a) (b)

Figure 9 (a)Verge assembly with the connecting square, two pallets to the side connected with bolts and the two 10x6x2.5 bearings. (b) Prototype version of the crown gear

2.4.3. Prototype

Due to the limitations in terms of manufacturing methods and budget, the crown gear and housing parts were made using a FDM 3d printer, hand tools and a simple 2.5D CNC mill. The verge and axles needed for the prototype were machined on conventional mills and lathes. For the means available, this resulted in a prototype closest to the production version possible with only the housing being 3D printed instead of machined in aluminium.

2.5. Numerical Simulation

The multibody dynamics package ADAMS uses the verge and crown gear from the previous section to simulate the dynamics of the system. The coefficient of restitution is not present in the ADAMS contact model. However, the following four parameters perform a similar function, and have to be chosen by the program user and should be found through experiments.

Contact stiffness k
Force exponent e
Maximum damping c_{max}
Penetration depth d

The contact stiffness says something about the geometry and materials, the force exponent describes the non-linearity of the spring force in the contact. The maximum damping can be found experimentally, or the standard ADAMS value of 0.01% of the contact stiffness can be used. The penetration depth is the depth at which this maximum damping is achieved, and should be chosen higher than the maximum expected depth (Giesbers, 2012). These parameters describe the transfer and dissipation of energy in the collision and is dependent on the geometry, materials and velocity of the components. A full description of the components can be found in Appendix 6.2.

2.6. Model verification and performance testing

The coefficient of restitution in the analytical model and the contact parameters in ADAMS have a big influence on the dynamics. Therefore, it was deemed necessary to engage in a performance testing to verify those models with prototypes and that way also help answer the research question:

Which parameters dominate the dynamic behaviour of the deployment?
Can analytical and numerical models accurately predict real world behaviour, considering production accuracy and tolerances?
Can those parameters be used to tailor the escapement to the variation of solar arrays it can encounter?

The main goals is to compare the extended model with the ADAMS program and the prototype. Through various variations of the prototype, the influence of design parameters will be investigated. The following tests will be done:

2.6.1. Design parameters

From the six phases, it can be concluded that the average rotational velocity is dependent on many factors. Some of which, are system properties such as the input torque, which is derived from the solar array requirements. To make this an useful product, the parameters that *can* be chosen freely are interesting to analyse further. There are a number of design parameters that have a significant impact on the rotational velocity, both adjustable and not. These parameters are:

- Number of teeth
  Three variants will be made and tested. One with 15, 21 and 27 teeth. (Figure 11)
- Inertia of Verge
  Two variants will be made and tested, one with 0.2 and one with 0.4 $kg\ mm^2$ (Figure 12)

Input torque
: Variation between 1 and 2 Nm

Long runs
: Many runs with one of the configurations to judge wear

2.6.2. Test setup

The test setup can be seen in Figure 10. The position data is recorded using hall sensors that measure the change in magnetic field of a magnet that is mounted on the end of the verge and crown gear (red circles). This measurement is recorded and later converted to degrees. The benefit of using these sensors is that there is no physical contact between the verge and the measuring device. The magnet has a negligible effect on the inertia of the verge and crown gear.

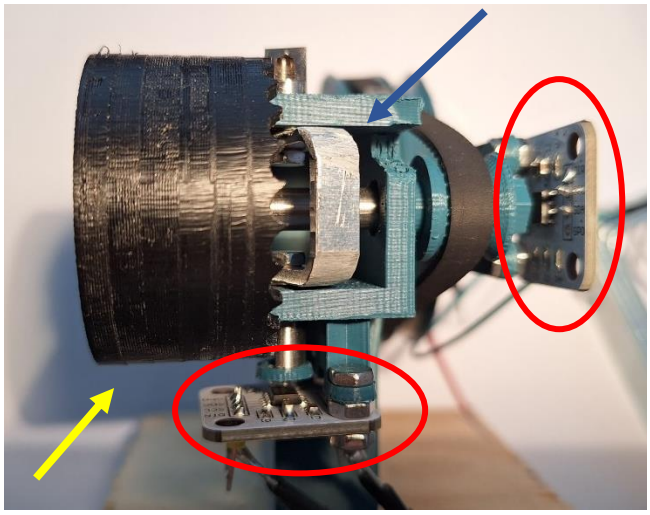

Figure 10 Test Setup, position sensors circled in red. Crown indicated by the yellow arrow, verge by the blue arrow.

Figure 11 Crown gears with, from left to right, 15, 21, 27 teeth

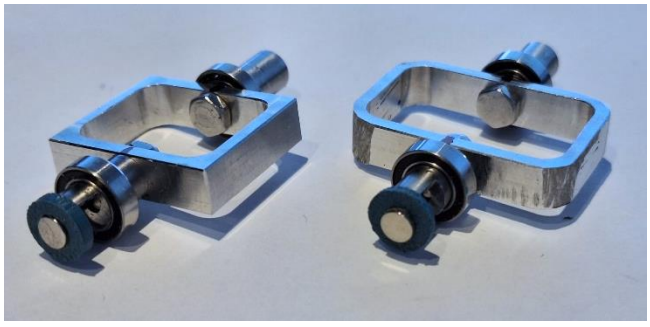

Figure 12 Verge variation with 0.25 and 0.4 kg mm^2

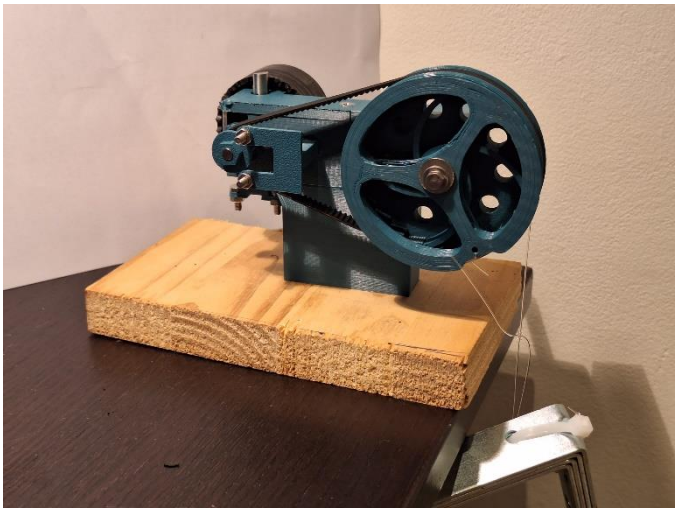

Figure 13 Test setup, weight hanging on the right, escapement on the left and 1:5 ratio wheels in between.

3. Results

In this chapter the results of the analytical and numerical simulations, as well as the results from prototype testing are shown. First, a comparison is made on the dynamics in a single interaction, of the mechanism. Then, the resulting revolutions per minute of the solar array is shown for all models.

3.1. Escapement Dynamics Results

The rotational velocity over time was analysed for all three data sources. The Extended model, ADAMS simulations and lastly the prototype testing. In Figure 13 the angular velocities of the crown and verge are visible for a few cycles. In this figure, the vertical lines indicate collisions, an near instantaneous change in velocity.

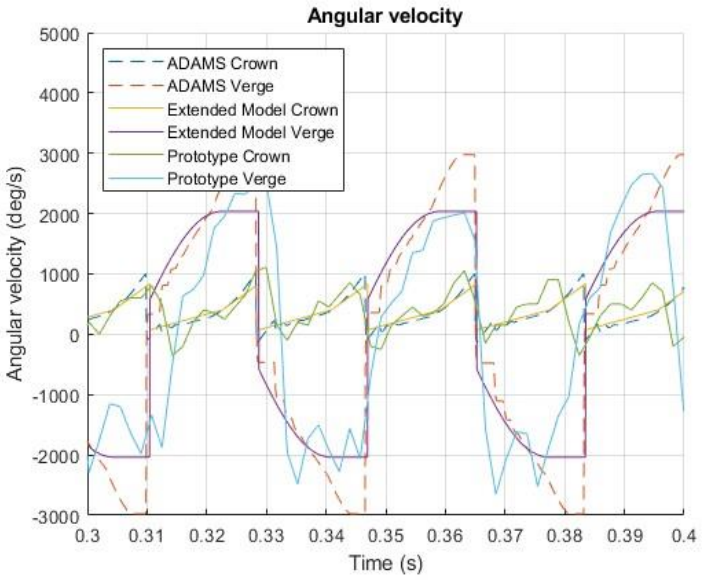

Figure 15 Adams/Extended model comparison

3.2. Parameter Variation

To investigate the influence of the parameters on the performance of the escapement, the most effective of the parameters were varied.
In the analytical models, the following:

Number of teeth $(N + 1)$ (Figure 17)
Verge Inertia (I_v) (Figure 19)
Input torque (τ) (Figure 18)
Crown gear radius (r_c) (Figure 16)

ADAMS and the prototype allowed for the variation of:

Number of teeth $(N + 1)$
Verge Inertia (I_v)
Input torque (τ)

The coefficient of restitution was kept constant between all measurements. For the Extended model this coefficient was $c_r = 0.165$, and for the Roup model $c_r = 0.3$. Unless mentioned otherwise, the inertia of the verge is $I_v = 0.41\ kg\ mm^2$.

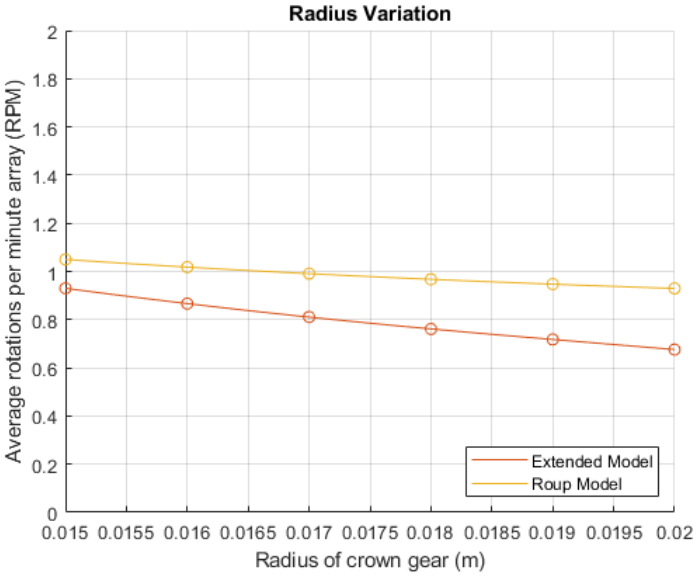

Figure 16 Variation in the parameter crown gear radius r_c from 15 to 20mm

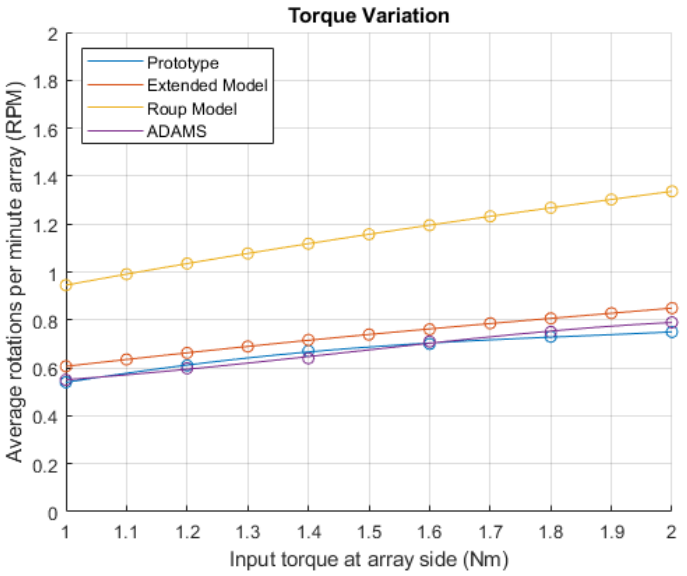

Figure 18 Variation in the parameter input torque from 1 to 2Nm

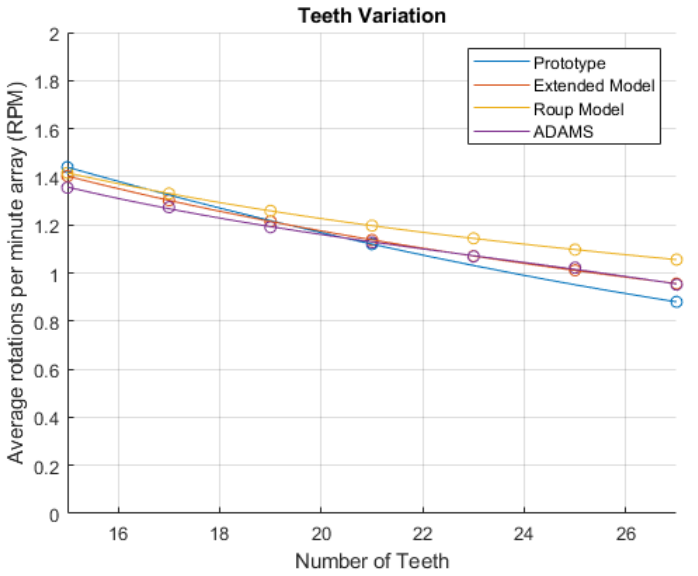

Figure 17 Variation in the parameter number of teeth from 15 to 27 teeth

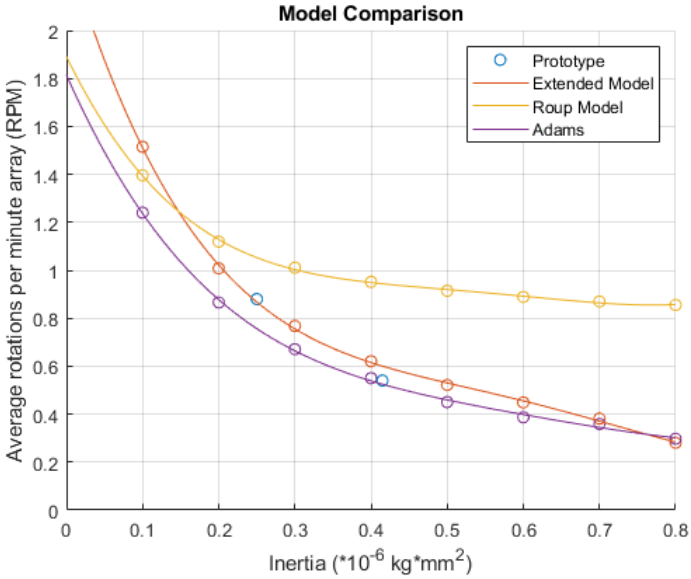

Figure 19 Variation in the parameter verge inertia I_v from 0.1 to $0.8kg\ mm^2$

3.3. Limit cycle

When running, the dynamics system displays stable and repetitive behaviour, a limit cycle. In the Roup-model, four of the aforementioned six phases are present; phase two, three, five and six. This cycle is illustrated in Figure 20. In the Extended model as well as ADAMS measurements, all six phases can be seen (Figure 21). This data is also available for the prototype, however was not of deemed of sufficient resolution to compare with these two datasets.

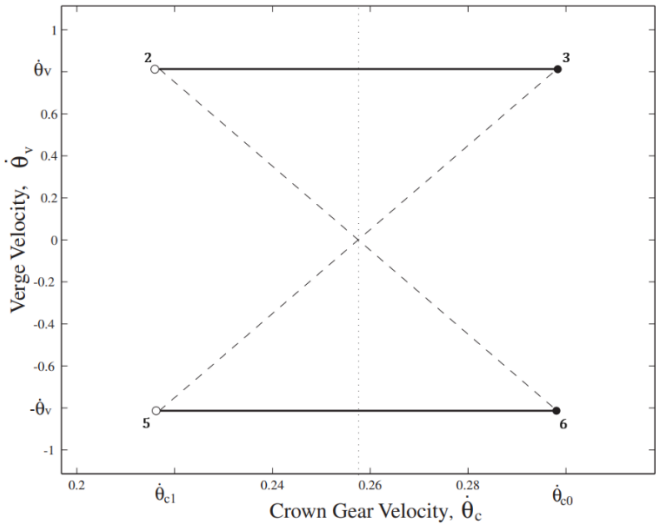

Figure 20 Velocity phase portrait of a representative periodic orbit. The numbers correspond to the start of the phases. The continuous-time trajectories are shown with solid lines and the impulsive jumps are shown with dashed lines.

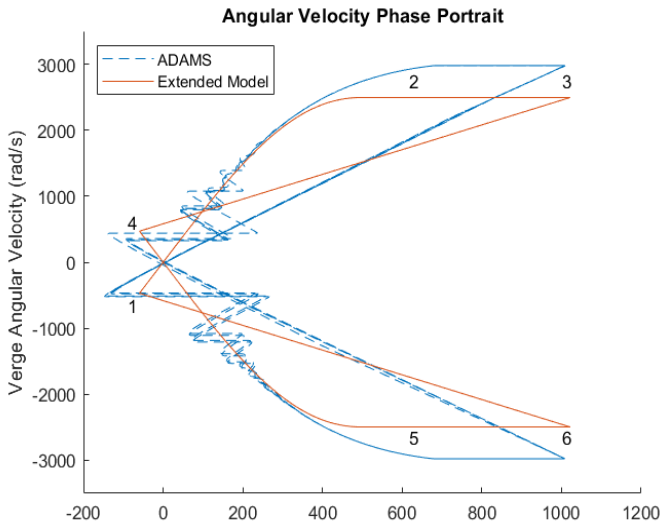

Figure 21 Velocity phase portrait of the periodic oscillations. The numbers correspond to the start of the phases.

3.4. Prototype testing

In Figure 22, the rotational velocity of the verge is visible that was measured with a laser interferometer to achieve higher data resolution. During this measurement, it was not possible to measure the rotational velocity of the crown at the same time.

Figure 23 shows a detailed view of the angular velocity of the verge. Multiple irregularities in the curvature are highlighted. Figure 24 shows a comparison between both the velocity and the position of the verge.

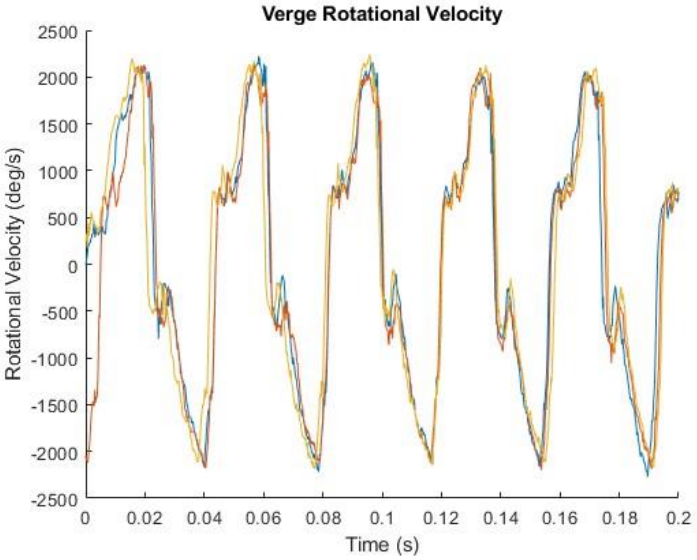

Figure 22 Verge linear velocity obtained using a laser interferometer perpendicular to the verge in neutral position, so looking down onto the crown gear. Hence, linear velocity.

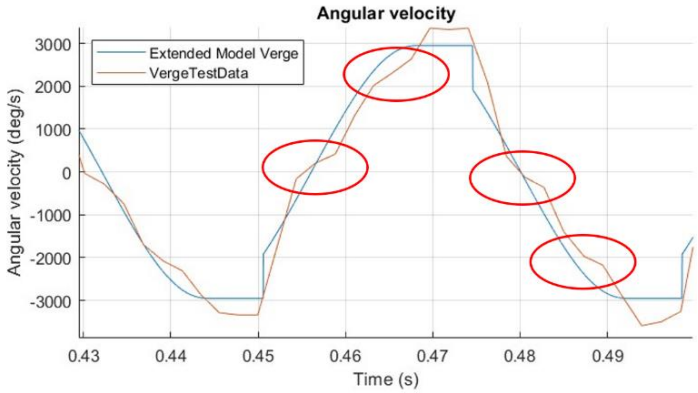

Figure 23 Single cycle verge angular velocity comparison. Irregularities in the curve are highlighted in red

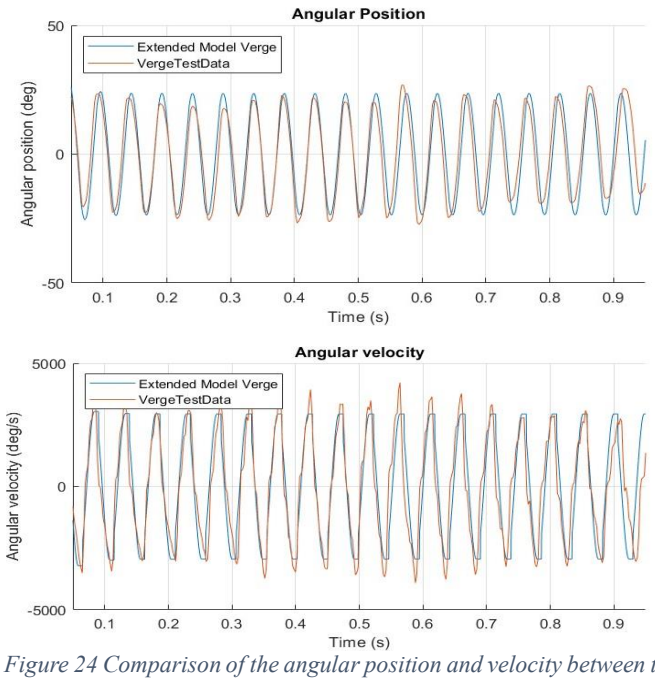

Figure 24 Comparison of the angular position and velocity between the experiment data and the extended model

3.5. Multiple panel simulations

A final analysis was done using ADAMS, and escapements were attached to a solar array consisting of three panels, to see the effect. Four tests were done with increasing numbers of escapements:

1. No escapements
2. Only on first hinge
   - Spacecraft – Panel 1
3. Root hinge and second hinge
   - Spacecraft – Panel 1
   - Panel 1 – Panel 2
4. Root hinge, first and second hinge
   - Spacecraft – Panel 1
   - Panel 1 – Panel 2
   - Panel 2 – Panel 3

The results are in the following table:

Test NR.	Time to deployed (s)	Highest latch shock (Nm)
1	10	25
2	54	11
3	50	8
4	51	5

Table 1 - Results deployment tests in ADAMS

4. Discussion

In this discussion, the results of the previous chapter are discussed. This will be done separately for the analytical models and the prototype tests. The Design will also be discussed. Afterwards the research questions are reviewed and conclusions drown. The chapter is finished with recommendations for next steps and improvements.

4.1. Analytical models for escapement performance prediction

To judge the performance of the analytical models, the results will be compared with the ADAMS results as well as the measurements obtained from the prototype.

4.1.1. Escapement dynamics

In Figure 15, (larger version visible in Appendix 6.4) when looking at the crown gear data from ADAMS and the Extended model, a distinct transition can be seen in the crown gear velocity. After the vertical jump in velocity, a curve transitions in a horizontal line. This is the moment where the verge and crown gear accelerate together, and afterwards the verge loses contact. This continuous acceleration is not present when using the model developed by Roup *et al.,* where only a discrete step in velocity is visible for the verge. This is happening during phase one and four. Then, the rate of acceleration increases for the crown gear while the velocity of the verge remains constant. What also can be noticed in the ADAMS data is the realistic situation of multiple collisions, indicated by steps in the rotational velocity of the verge. Since the collision will have a $CoR > 0$, the two bodies will move apart from each other after the impact. Then the crown gear will accelerate and catch up, resulting in ever smaller collisions until finally the verge maintains contact with the crown gear.

The difference between non-extended and extended versions of the continuous-discrete hybrid model becomes even clearer when looking at the angular velocity phase portrait as seen in Figure 3 of Roup *et al*. This figure is copied and visible here as Figure 20. There is no interaction between the two bodies apart from the collisions resulting in the straight lines. Figure 21 shows once again the difference of having multiple real-world inelastic collisions in which some kinetic energy is dissipated in the ADAMS model and the continuous lines of the extended model.

The differences in dynamics is taken into account by the coefficient of restitution. The model is tuned by adjusting the coefficient of restitution until all graphs match the ADAMS and prototype data as close as possible. Therefore these differences in detail, visible when looking at the limit cycle, become nearly unnoticeable when comparing average rotational velocity of the crown gear or solar array.

4.1.2. Average Rotational Velocity Prediction

The average rotational velocities are visible in Figures 16-19. These, it is visible that the analytical models can quite accurately predict the impact of parameter variation. Especially the variation in the inertia of the verge (Figure 19) shows that the addition of phase one and four is needed to predict the performance at higher inertias. The other variations show that the additional phases make sure that the coefficient of restitution does not have to be changed when varying the parameters. If one would try to match the results of the Roup model to the ADAMS and prototype measurements, the coefficient would range from 0.1 to 0.48 depending on the variable.

4.1.3. Model Simplifications

To make the system of equations, some simplifications have been made. These simplifications were made to stay away from trying to make a full contact model which is outside of the scope of this paper. The main goal of the analytical approach was to get an accurate enough estimation of the average rotational velocity of the crown gear to prevent having to make many 3d models to simulate using ADAMS. This was achieved using the following simplifications.

Collision, measurements and torques implemented in 2D only

Due to the localized nature of the collisions this has been implemented as it were a 2D collision. In reality, the verge never collides while the pallet is perfectly vertical. Also, the bodies rotate around an axle and are not translating linearly. The local velocity vector of the verge and crown gear are assumed to be directly in line with each other and tangent to the radius of the crown gear.

No contact model

Different from ADAMS, the analytical solution does not allow for a full contact model with the use of parameters like contact stiffness, damping and penetrations depth. All these parameters are left out.

Simplified situation after collision

After the collision the verge is modelled to stay in contact with the crown gear, as a fully in-elastic collision, which is unrealistic as explained previously. This is done to allow for the jump criteria to be implemented and changed more easily. Furthermore, if this contact was implemented more realistically, the timesteps used in the calculations should have been (much) smaller. This increases calculation time, reducing the advantage of the extended model. Especially since this fact does not seem to impact the accuracy of the model, except at maybe lower inertia's (Figure 19) since the verge would have carried more velocity after the collision.

Implementation of the coefficient of restitution

To compensate for absence of contact model, situation after collision, other inaccuracies, and most importantly, to allow the system to dissipate energy. In a real world scenario, the collision would result in wear, heat, sound and vibrations all subtracting energy from the system, slowing the rotation down. Without this, the mechanism would keep accelerating and not enter its limit cycle. This value is chosen by comparing the outcome of the extended model with many simulations done in ADAMS. This way, the contact model with damping, geometry and elastic behaviour of the collisions is compensated for in the coefficient. For the extended model , it equals $e = 0.165$

4.2. Prototype Performance Review

Similar as to the analytical model reviews, first the dynamic data is discussed and afterwards the rotational velocity of the crown gear and therefore solar array. Finally a short review of the wear observed during the prototype testing.

4.2.1. Position data Comparison

The performance tests resulted in the data on the rotational position of the verge, from which the rotational velocity could be calculated. The rotational velocity comparison between the extended model and the experiments can be seen in Figure 24. When comparing these two datasets, the adjusted residual squared can be calculated and equals: $R^2_{Adjusted} = 79.5\%$.

When comparing a single cycle it can be seen that the angular velocity seems constant at multiple points in the cycle. This can be seen in Figure 23 and is indicated with red circles. This would mean that there are multiple bounces between the verge and the crown gear. This is also what ADAMS predicted, and was mentioned when comparing ADAMS and the analytical models.

4.2.2. Variable variation comparison

Number of teeth

The results of the tests show that changing variables have predictable consequences for the variation in the number of teeth. More teeth on the crown gear resulted in a slower rotational velocity for the escapement. In the Figure 17 it can be seen that the extended model underestimates the effect of these changes. For 15 teeth the prototype rotated ~5% faster on average and for 27 teeth the prototype rotated ~10% slower.

For these tests the inertia of the extended model was matched to the prototype. The distance between the verge and the crown gear was measured and adjusted as accurately as possible, however still had some variation. For the 27 teeth the distance was 1.93mm, for 21 1.96mm and for 15 2.01mm where 2mm was the distance aimed for. This distance was measured before and after each test and averaged. Finally, the average speeds were measured after the initial startup behaviour when velocities were stable.

Inertia of verge

For the inertia a similar picture can be seen, with the larger inertia of the verge resulted in slower angular velocity, which was also predicted by ADAMS and both analytical models.

Input torque

In these tests it became clear that the prediction that input torque has a non-significant effect on the rotational velocity. However, the contact forces at the maximum torque proved too much to handle for the gear with the smallest amount of teeth, 15. This wear will be discussed in 3.3.

4.2.3. Wear

For the mechanism, a 90 degree rotation of the solar array means 20 rotations of the crown gear at a 1:80 gearbox. This would be for a root hinge, other hinges rotate 180 degrees. At the moment of writing, the 27 tooth gear has performed around 135, 90 degree panel deployments without a sign of significant wear. However, the 15 teeth gear prototype has shown a peculiar failure mode that is probably a direct consequence of the manufacturing method.

From the damaged prototype it can be seen that one tooth has sheared off. It is evident that this has happened at the interface between two layers of the 3d printed part. The 3d printed PETG is known for its good layer adhesion. Further tests should point out if this failure is only caused by the manufacturing method or if the forces are simply too high.

4.3. Design Review

This section describes additional consideration concerning the design.

4.3.1. Thermal

The large delta between the highest and lowest possible temperature means that polymers experience significant expansion and contraction during these thermal cycles. On the interface between the polymer and metals, this could result in stresses when fastened with bolts for example, when the fit is too tight. It also means that the radius for the crown gear should be chosen such that under the highest temperature, it does not interfere with the surroundings. Under both the highest and lowest temperature, the gear should interact with the verge. Alternatively, the mechanism could be protected from the sun using a thin heat blanket, preventing these problems entirely.

4.3.2. Flow of energy

There are two possibilities to power this mechanism, either from the hinge side a strong torque spring that powers the deployment, and gets reduced through the gearbox until it arrives at the escapement. The other possibility is to use a constant torque spring at the escapement side of the system that can provide a constant torque for the 20 rotations it has to unwind. That way potential friction in the mechanism does not get magnified through a gearbox before it arrives at the spring on the hinge side.

Due to the mechanism having quite a constant velocity under a variation of torques, it seems like no problem to have the spring on the hinge side of the system, like it is in the current hinge design. The hinge still has to be changed to allow for the mounting of the system, but the spring assembly can then be maintained. This would mean the escapement can act as an add on to normal Sparkwing hinges. This would be ideal, since when during the design process, or even manufacturing process it turns out the requirements change or the velocity is greater than expected, the escapement can still be added.

4.3.3. Manufacturing

The manufacturability of the design was taken into account when designing the prototype. During manufacturing it showed that it could be made with basic tools. Nevertheless, it involved quite a bit of manual labour that might turn out expensive for mass production. Processes such as 3D printing metals or even casting and finishing on a mill, might be beneficial to look into for larger production runs.

For the crown gear, the teeth can be machined on a 3-axis CNC mill, and for PEEK that seems like the most suitable manufacturing method. The fact that the mechanism performs under worse manufacturing tolerances and rudimentary production methods, shows that the system is quite insensitive to inaccuracies in that regard. It should be kept in mind that the products in the space industry are never produced on a scale that rule out more sophisticated production methods.

4.4. Escapement Performance Summary

In this paper a numerical model was derived to predict the performance of future escapement designs for Airbus NL. This model was used to estimate design parameters for an escapement to reduce the rotational velocity of solar array deployments.

It was shown that the extended model could predict the performance of escapements and this was verified using experiments. The hybrid nature of the continuous-discrete model provided correct trends in terms of variation in design parameters. The fact that a constant coefficient of restitution provided values close to reality for all configurations makes it a useful tool and an improvement over previous academic work.

The prototype functioned as expected, and was relatively easy to assemble and tune. The final prototype could be considered complete in terms of manufacturing quality and under those conditions the mechanism was always self-starting and never got stuck, two of the most important requirements. The failure on the 15 teeth gear should be further investigated to see if this also happens for isotropic materials. The results visible in Table 1 give confidence the mechanism can reduce latch shock.

4.5. Conclusions

- Escapements proven to be a viable option to control solar array deployments
- Resulting rotational velocity can be adjusted such that it is between 0.16 and 1.5RPM
- Performance can be predicted using ADAMS and numerical models.
- Components can be modified to adjust the desired performance
- Can be produced within the main requirements of section 2.1

4.6. Future development/recommendations

The current study can be seen as the ground work for this new concept to build upon. It should give confidence to push on with the concept since the calculations and tests suggest it could work well. However, some more testing should be done before fully developing this product into a space worthy component

The first thing I would recommend doing is to design and manufacture a simple hinge, on which the mechanism including gearbox can be mounted. Assuming the gearbox can readily be chosen. This doesn't need to have an array attached in the beginning, but wiring and springs and all other components contributing to friction and torque need to be there. Then the mechanism can be tested fully. Most interesting would be the influence of the inertia of the gearbox and the play in the gearbox. The inertia of the arrays can then be simulated on the mechanism using a simple weight for example. That way it is possible to provide a more realistic testing environment and further verify the work done for this paper. This 'dummy' array would be a step after that. Then, the product should be ready for integration.

The risks that these test would mitigate are: unknown complications from adding the gearbox. The gearbox adds an unknown amount of friction, inertia and play into the system. Until now, the torque was applied directly to the mechanism, not through a gearbox. The flexible multibody behaviour of a dummy array would be interesting to see if that has an effect in increasing, and decreasing the torque on the mechanism.

Furthermore, the verge should be contained that it cannot rotate more than +/- 30 degrees to prevent the mechanism getting stuck. A solution should be found to repack the array after testing a deployment, currently the concept is not back drivable.

5. Bibliography

Ali-Akbari, H. R. (2018). *Design of a Satellite Solar Panel Deployment Mechanism Using the Brushed DC Motor as Rotational Speed Damper.* International Journal of Aerospace and Mechanical Engineering.

Cipolla, C. M. (2003). *Clocks and Culture 1300-1700.* New York City: W.W.Norton & Company.

Doejaarden, F., & Ellenbroek, M. (2012). The Damper Unit of the Sentinel 1 Solar array. *Aerospace Mechanisms Symposium.* Pasadena, CA.

Giesbers, J. (2012). *Contact Mechanics in MSC ADAMS.* Enschede: University of Twente.

Kroon, M. (2022). *SBIR Eindrapport Fase 1.* Leiden: Airbus NL.

Lepschy, A., Mian, G. A., & Viaro, U. (1992). Feedback Control in Ancient Water and Mechanical Clocks. *IEEE Transactions on Education, 35*(1), 3 - 10.

Nunez, Á., Pérez, C., Maldonado, A., Plaza, M., & Cespedosa, F. (2003). *A SPACE QUALIFIED MECHANICAL SPEED REGULATOR FOR DEPLOYABLE DEVICES THAT PROVIDES SPEED CONTROL WITHOUT ELECTRICAL POWERING OR COMMANDING.*

Roup, A., & al., e. (2001). Limit cycle analysis of the verge and foliot clock escapement using impulsive differential equations and Poincare maps. *International Journal of Control*, 3245-3250.

Starkovich, J. A., Shtarkman, E. M., & Rosales, L. A. (1997). *United States of America Patent No. 5,921,357.*

Weir, G., & McGavin, P. (2008). The coefficient of restitution for the idealized impact of a spherical, nano-scale particle on a rigid plane. *Proceedings of the Royal Society A: Mathematical, Physical and Engineering Sciences*, 1295–1307.

6. Appendix

6.1. Additional Requirements

- The mechanism shall be self-starting
- The mechanism shall be designed for 200 deployments on ground and 1 in orbit
- The escapement mass shall be less than 100g
- The escapement shall fit within a cylindrical volume 40mm in diameter and 25mm in length.
- The escapement shall be able to withstand a shock load of 0.25Nm
- Acceptable deployment rate lies within 0.16RPM and 1.5 RPM at the array side
- Static friction, measured as a torque input, of the escapement shall be less than 0.01Nm
- The escapement mechanism shall be able to survive a qualification temperature range between -150°C (TBC) and +150°C (TBC)
- The escapement mechanism shall be able to operate in a qualification temperature range between -40°C and +150°C

6.2. Changes to Collision Trigger

While going through extending the analytical model, it was found that the calculation of distance was done in a peculiar way in $\mathcal{S}$:

$$r_c * \sin(x_1 - m\alpha_c) = r_v \tan(x_2 + \frac{\alpha_v}{2})$$

The left part of the equation (21 in (Roup & al., 2001)) is straightforward, it calculates the distance 'a' or 'b' (depending if the collision happens before or after the neutral line (yellow) between the gear tooth and the neutral line, viewing the crown gear from the top:

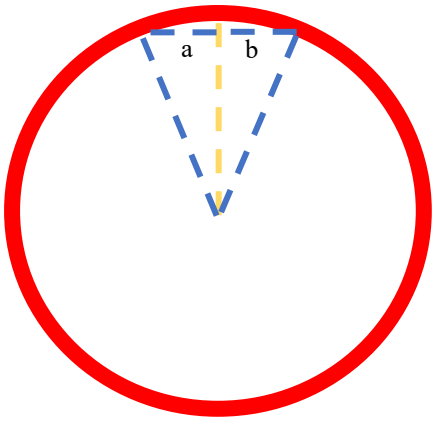

The right side of the equation should calculate the horizontal distance (a or b - red) of the contacting surface of the verge to the neutral line, if it wants to calculate the collision distance. But it calculates the distance perpendicular to the verge (c - red) resulting in a small difference. Furthermore, it can only calculate the distance correctly if the contact happens at the tip of the verge (right figure). For the left figure, the distance should be calculated with the height of the verge, not the length resulting in distance d (green) (Hv instead of Rv). These are the two reasons there are now four contact condition accounting for the two situations below for both the upper and lower verge.

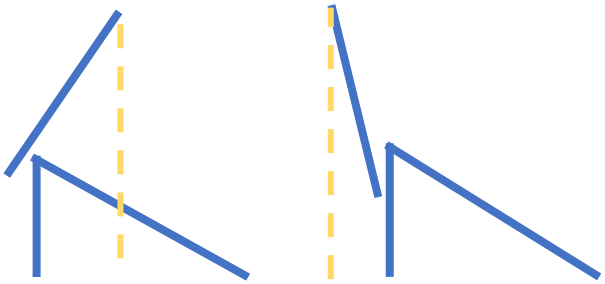

6.3. Contact Parameters ADAMS

The following information regarding the ADAMS contact model comes from chapter 4.2 from a bachelor's assignment by Jochem Giesbers (2012). This information was obtained through experiments in ADAMS with a bouncing ball and other academic sources.

6.3.1. Stiffness k:

Even though the name stiffness might sound like it is a material property, it is not just that. It also depends on the geometry of the colliding objects. Therefore there is no documentation for choosing the value for k. The best option is to do multiple simulations in Adams with different values of to determine the optimal value, the value at which the Adams contact behaviour resembles the real world contact behaviour.

6.3.2. Force exponent e:

The force exponent is a measure of the non-linearity of the IMPACT function's spring force. In Chapter 2.6 it was already explained that the recommended value is , because lower values will lead to discontinuities when IMPACT activates. The actual value of e is a material property. Soft materials, like rubbers, have a force exponent of e = 1.1. For harder materials, the force exponent increases. Soft metals, like aluminium, a force exponent of $e = 1.5$ and hard metals, like steel, have a force exponent of $e = 2.2$.

6.3.3. Maximum damping c_{max}:

Some sources say that it is recommended to have a maximum damping coefficient that is 1% of the stiffness value. Experienced users believe that should be even smaller. In Adams, the standard stiffness is $1 * 10^8 N/m$ and the standard maximum damping coefficient is $1 * 10^4 N * s/m$, which is 0.01% of the stiffness value. The best option is to do multiple simulations in Adams with different values of to determine the optimal value, the value at which the Adams contact behaviour resembles the real world contact behaviour.

6.3.4. Penetration depth d:

This penetration depth is not the maximum penetration depth, but the measure of how the damping coefficient ramps up from zero to c_{max}. The value should be smaller than the expected maximum penetration depth. A reasonable value for this parameter is 0.01mm.

6.4. Larger Figure

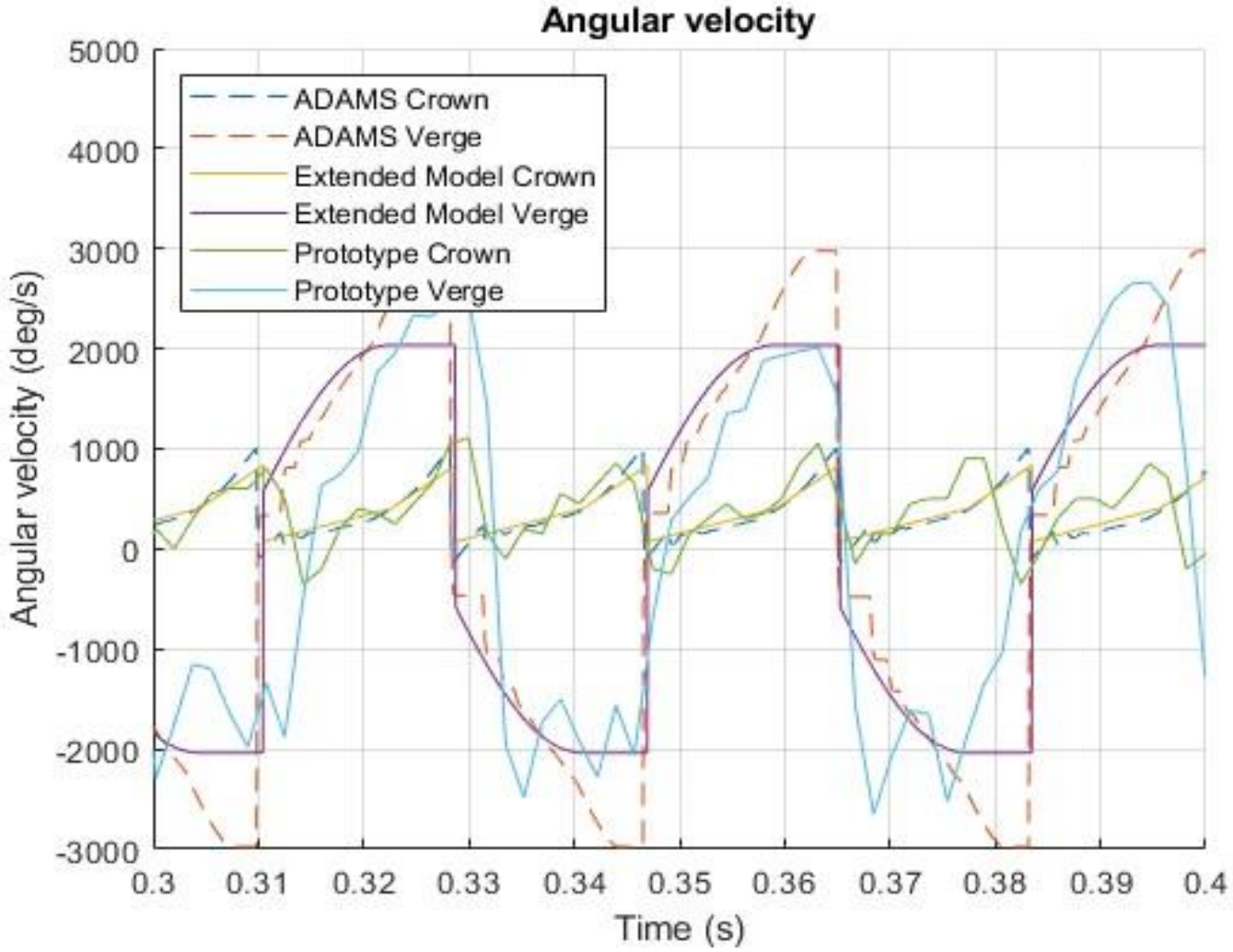

Figure 26 Adams/Extended model comparison